Photoacoustics 25 (2022) 100316

Contents lists available at ScienceDirect

Photoacoustics

journal homepage: www.elsevier.com/locate/pacs

Algorithms for optoacoustically controlled selective retina therapy (SRT)

Eric Seifert [a,*], Jan Tode [c], Amelie Pielen [c], Dirk Theisen-Kunde [a], Carsten Framme [c], Johann Roider [b], Yoko Miura [a,d], Reginald Birngruber [d], Ralf Brinkmann [a,d]

[a] Medizinisches Laserzentrum Lübeck GmbH, Peter-Monnik-Weg 4, 23562 Lübeck, Germany
[b] Klinik für Ophthalmologie, Universitätsklinikum Schleswig-Holstein, Arnold-Heller-Straße, 24105 Kiel, Germany
[c] Universitätsklinik für Augenheilkunde, Medizinische Hochschule Hannover, Carl-Neuberg-Str. 1, 30625 Hannover, Germany
[d] Institut für Biomedizinische Optik, Universität zu Lübeck, Peter-Monnik-Weg 4, 23562 Lübeck, Germany

ARTICLE INFO

Keywords:
SRT
Lasers in medicine
Ophthalmology
RPE
Selectivity
Algorithm
Retina therapy
Optoacoustics
Feedback

ABSTRACT

Objectives: Selective Retina Therapy (SRT) uses microbubble formation (MBF) to target retinal pigment epithelium (RPE) cells selectively while sparing the neural retina and the choroid. Intra- and inter-individual variations of RPE pigmentation makes frequent radiant exposure adaption necessary. Since selective RPE cell disintegration is ophthalmoscopically non-visible, MBF detection techniques are useful to control adequate radiant exposures. It was the purpose of this study to evaluate optoacoustically based MBF detection algorithms.
Methods: Fifteen patients suffering from central serous chorioretinopathy and diabetic macula edema were treated with a SRT laser using a wavelength of 527 nm, a pulse duration of 1.7 µs and a pulse energy ramp (15 pulses, 100 Hz repetition rate). An ultrasonic transducer for MBF detection was embedded in a contact lens. RPE damage was verified with fluorescence angiography.
Results: An algorithm to detect MBF as an indicator for RPE cell damage was evaluated. Overall, 4646 irradiations were used for algorithm optimization and testing. The tested algorithms were superior to a baseline model. A sensitivity/specificity pair of 0.96/1 was achieved. The few false algorithmic decisions were caused by unevaluable signals.
Conclusions: The algorithm can be used for guidance or automatization of microbubble related treatments like SRT or selective laser trabeculoplasty (SLT).

1. Introduction

1.1. Laser treatment of the retina

Retinal laser treatments are standard of care for a variety of posterior segment ocular diseases. The retinal pigment epithelium (RPE) is a monocellular layer between the photoreceptors and the Bruch's membrane where 20–80% of the incoming light is absorbed [1–3]. Using treatment pulse duration above 50μs thermal damage is dominant for laser radiant exposure close above damage threshold [3,4]. For pulse durations in the lower microsecond ($\leq 2\mu s$) and nanosecond regime, RPE cell damage is induced by intracellular microbubble formation (MBF) [5,6]. Microbubble formation leads to a disintegration of the cell structure, including the cell membrane, while sparing the photoreceptors [5,7]. Hence, selective damage is especially useful for patients with impaired RPE function. In the healing period after laser treatment the increased metabolism at the choroidal junction leads to the impression of a rejuvenated RPE. Beneficial effects of selective RPE damage were proven after treatments of central serous chorioretinopathy (CSCR) [8–11] and diabetic macula edema (DME) [12,13].

To reduce the risk for photoreceptor damage it is required to treat close above the MBF threshold. However, intra- and inter-individual variations in the fundus pigmentation [14] and the transparency of anterior eye media [15] lead to varying pulse energy settings needed to achieve initial MBF at the RPE. Furthermore, selective RPE damage is non-visible for the treating physician.

Timely and costly treatment protocol including additional diagnostic procedures are demanded to verify RPE damage, like includes fluorescence angiography (FA) with fluorescein or indocyanin green. FA is typically used to demarcate neovascular areas, but also regions where the blood-retina barrier is not intact, e.g. for pathologic changes or in regions of damaged the RPE, like after laser irradiations. In the latter case the fluorescein molecules can pass through the broken tight junctions between the RPE cells and becomes visible as bright spots after

* Corresponding author.
E-mail address: seifert@mll.uni-luebeck.de (E. Seifert).

https://doi.org/10.1016/j.pacs.2021.100316
Received 6 August 2021; Received in revised form 19 October 2021; Accepted 9 November 2021
Available online 10 November 2021

excitation by the FA system [16–19]. Even though FA became a standard procedure, costs, time, and adverse effects like allergic reactions [20,21] make it unattractive to apply in the clinical daily use. The FA images only be acquired a few seconds after the injection of the fluorescent dye (early phase) in order to clearly demarcate the laser areas. Due to the time the body needs to remove fluorescein from the body, FA can be applied once a day only. Thus, FA is not suited for an iterative laser dosing during a treatment procedure.

1.2. Microbubble detection techniques

In order to make FA abdicable, other techniques to demark RPE damage are desirable. Such techniques shall be applicable best during treatment, not after treatment.

Optic techniques including interferometry, optical coherence tomography and evaluation of backscattered light were introduced to detect MBF as an indicator of RPE cell damage [9,13,22–32]. MBF also generates acoustic waves during expansion, which can be measured with an ultrasonic transducer embedded in a contact lens, a standard tool in retinal laser treatment. Thus, an algorithm which can reliably determine optoacoustic signals originating from microbubbles consequently also predicts cell damage. The advantage of optoacoustic techniques lies in the independence of acoustic signals from light scattering within the eye, especially relevant for older patients. While optical approaches may not be applicable at a certain degree of glaucoma optoacoustic techniques may still work.

The disadvantage of the optoacoustic method from Schuele et al. is that this algorithm compares all transients from one spot and evaluates transient differences in order to separate thermoelastic from MBF related transients [33]. This algorithm strategy, however, can reliably detect MBF after irradiation, but is not compatible with an automatic irradiation procedure with increasing laser pulse energy. Further, suitable algorithms must be independent of the pressure amplitude from both, the applied laser pulse energy and the location within the eye, especially the angle to the ultrasonic transducer.

With the development of SRT-Laser systems which include techniques to acquire optoacoustic pressure transients, like the R:GEN system (Lutronic Corp, Republic of Korea), there is a growing interest in finding an adequate safe and reliable algorithm with high sensitivity and specificity to identify microbubbles with acquired pressure transients in order to automatically control the laser application. It is the purpose of this work to develop and test an algorithm which is designed to discriminate individual optoacoustic pressure transients with and without signs of MBF, independent of the pulse energy and other limitations. It shall be suitable for an automatic spot individual irradiation ceasing after MBF detection during irradiation procedure with a pulse energy ramp.

2. Material and methods

2.1. Laser and optoacoustic detection

In this study, the R:GEN SRT-System (Lutronic Corp., Republic of Korea) was used. This system was based on a frequency doubled Q-switched Nd:YLF laser (527 nm) for treatment (Fig. 1a). The pulse duration was set to 1.7 µs and 15 pulses were applied with a repetition rate of 100 Hz. A pulse-wise increase of the laser pulse energy was implemented. This pulse wise increase in laser pulse energy is referred to as ramp. The starting energy was set to 50% of the maximum energy (E_{max}). The value of E_{max} was adjusted by the clinician before each irradiation. Since the pulse energy increases linearly, the pulse energy step size was 3.57% of the maximum energy. All 15 pulses were always applied to each spot, and E_{max} was reached at the 15th pulse.

The treatment light was guided to the irradiation unit (Fig. 1b) via an optical step index fiber with a core diameter of 50 µm and a numerical aperture of 0.11. Spatial irradiance variations within the beam profile

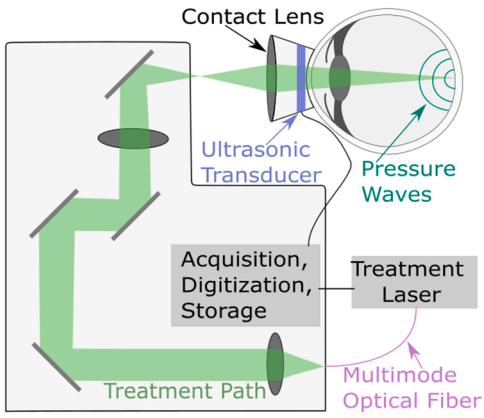

Fig. 1. Schematic of the clinical setup with (a) treatment laser and (b) irradiation unit.

were measured. A peak-to-mean ratio of 3.5 (Intensity Modulation Factor, IMF) was evaluated. A contact lens (R:GEN contact lens, Lutronic) was used. The spot diameter at the retina was set to 200 µm.

A disposable ultrasonic transducer was attached to the contact lens. The acquired pulse was digitized with a sampling frequency of 100 MS/s and an effective resolution of 14 bit. The acquired sensor data and information, such as pulse energy, was stored.

2.2. Clinical study and treatment

Nineteen treatments on 15 eyes of 15 patients (10 males and 5 females; average 54 years old, ranging between 35 and 76 years old) with symptomatic CSCR (11 patients) and DME (4 patients) were performed in this study. The 19 treatments also include four retreatments which were performed if no reduction of subretinal fluid or edema was found in the follow up observations. The study was conducted at the eye clinics of the University Hospital Schleswig-Holstein (UKSH) campus Kiel and Hannover Medical School (HMS). The procedures in the study adhered to the tenets of the declaration of Helsinki and its later amendments. The protocol and informed consent forms were compliant with and approved by the local institutional/ethical review boards (ethic committee vote number of HMS: 7393 and UKSH: B577/16).

At the beginning of each treatment, titration irradiations (also called test spot irradiations) were applied near the arcades. The position and maximum pulse energy were recorded for each spot. The maximum laser pulse energy (E_{max}) was increased by 10μJ for every second spot. The lowest E_{max} was 30μJ. This process was stopped as soon as ophthalmoscopically visible effects were observed. The E_{max} value used for the treatment was set to 80% of the energy of the first ophthalmoscopically visible spots. To ensure selective RPE damage in the treated area and to document the state of the RPE in the test spot area, FA was performed within one hour after treatment.

The acquired sensor data and additional information (e.g. laser pulse energy) were pseudonymously stored and utilized for analysis after the completion of the study.

2.3. Differentiation algorithms

2.3.1. Non-linearity (NL) detection algorithm

Several test and safety processes were executed before the primary microbubble detection calculations began. If a digital saturation was detected, if a signal was exceedingly low, or if signal disturbances were detected by those safety routines, the signal was not evaluated.

If the sensor-signal was rated as evaluable, the signal was filtered via a bandpass filter. The filter settings were automatically optimized, and its values are presented in the results chapter.

The generated pressure p is proportional to the radiant exposure H,

the absorption coefficient, and the temperature dependent Grüneisen coefficient $p(T) \sim \mu_a H\Gamma(T)$ [34,35]. The material specific Grüneisen coefficient is defined by $\Gamma(T) = \nu(T)\beta(T)/c(T)$; with the expansion coefficient β, speed of sound ν and heat capacity c. In the present setup, the temperature expansion dependent pressure generation is dominated by the radiant exposure H, and thus by the laser pulse energy E. The Grüneisen coefficient increases only slightly since heat accumulation is kept low by the low repetition rate to obtain selective damage.

During the irradiation of a single spot the laser pulse energy is ramped up. Thus, the maximum pressure increases with every pulse. In the acquired pressure transient data, this thermo-elastic increase was eliminated by normalizing the digitized transient p(t) to the laser pulse energy. The energy normalized pressure-equivalent δ was evaluated for each pulse. The ratio of δ_n (δ of the nth pulse) and δ_1 defines the *NL*-value.

$$\delta_n = \frac{\int |p_n(t)|dt}{E_n} NL = \frac{\delta_n}{\delta_1}$$

The Grüneisen coefficient was assumed to be constant since the low repetition rate of 100 Hz minimizes temperature accumulation. The NL value is around one in the case of no bubble formation and larger than one in the case of microbubble formation.

Since the presented algorithm makes use of the first thermoelastic transient for its local calibration, it can be speculated that any kind of cell damage (coagulation or microbubble formation) can make this calibration invalid. To work around this risk an additional heuristic has been applied: The NL-value can only be equal or higher than the previous NL value at a particular irradiation. This heuristic has also the side effect, that the optimization procedure becomes more sensitive to cases where an undamaged region is falsely identified as a damaged region (false positive). Since it is very important to avoid those false positives additional techniques to avoid those were presented in later chapters (Fig. 2).

2.3.2. Baseline algorithm

In one publication the optoacoustic algorithm used in the R:GEN device is described with the processing steps: 1 Offset removal, 2 Rectification, 3 Summation, 3 Error Check [36]. A normalization process is not mentioned for the optoacoustic signal processing. Thus, absorption differences and transducer angular sensitivity are not considered [36]. The exact algorithmic hardware implementation by Lutronic is not released in the literature.

It is good practice to compare a new algorithm being tested to an alternative method that is either the standard of practice or the easiest algorithm imaginable. In this work, an algorithm was applied that matches the published processing steps used by the RGEN system. This baseline algorithm (*BL* algorithm) makes use of the fact that optoacoustic pressure amplitudes tend to be higher in the case of MBF. In order to leverage this phenomenon, the BL algorithm summed up the absolute values of each pressure transient $p(t)$ with a minimum of preprocessing (DC offset removal only). Error detection included the detection of saturated signals, and signal amplitudes were too low to be labeled. This does not need to be identical to the implementation in the RGEN system.

$$BL = \sum |P_n(t)|dt$$

Fig. 3 displays the process flow of the BL algorithm.

2.3.3. Optimization procedure

Several settings of the algorithm described in the previous chapter were mentioned but not quantified. The values of those settings were found by an automatic optimization procedure. The automatic optimization procedure was a gradient descent process which maximized the area under the receiver operating characteristic curve (details in chapter 2.5).

This type of optimization belongs to a subcategory of machine learning procedures called supervised learning procedures. Those processes require labeled data for the optimization / training process. It is good practice to do optimization, threshold selection and testing with separate datasets, where no data in one dataset can be found in another. The difference between performance metrics of two datasets is a measure of the degree the algorithm or the threshold selection is overfitted to a dataset. The labeling / classification process, the datasets and the performance metrics are described in the following chapters.

2.4. Classification

To test whether the algorithm detects MBF correctly, all acquired transients were labeled in terms of presence (OA-positive) or absence (OA-negative) of microbubble induced increase in pressure amplitude. Fig. 5a displays an example OA-positive example (green transient) and Fig. 5c displays an OA-negative example (red transients only).

If it was not possible to make a classification (e.g. due to a low signal or noise level), the data received the label unknown. Date with the label unknown were not used. Since OA-transients can only be evaluated relative to each other, the first pulse cannot be classified, neither by a researcher, nor by the NL algorithm. Classification of optoacoustic signals was done for both the test and treatment spots.

The algorithm optimized to detect microbubbles shall also be used to detect cell damage. Thus, each documented test spot which could be verified by fluorescence angiography received a cell damage label.

Fig. 4a displays a FA image taken days before treatment, Fig. 4b displays a color image taken before treatment with notes taken during treatment, and Fig. 4c displays a FA image taken after treatment. If there

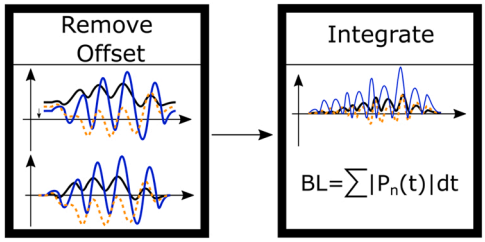

Fig. 3. Processing steps of BL algorithm include offset removal, rectification, summation, and an error check [36].

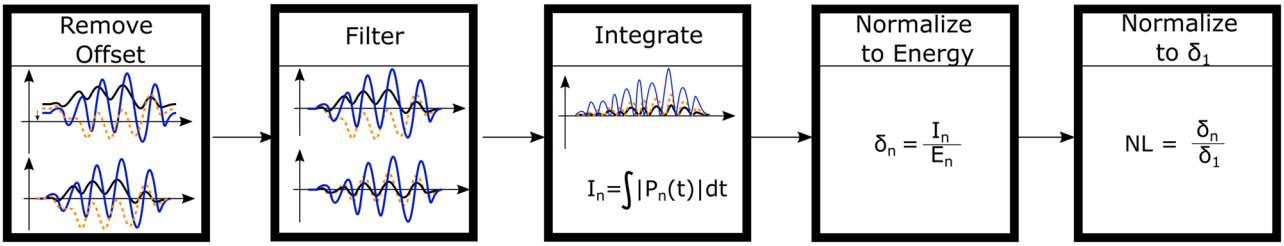

Fig. 2. Processing steps of NL algorithm include offset removal, filtering, rectification, integration, normalization and an error check.

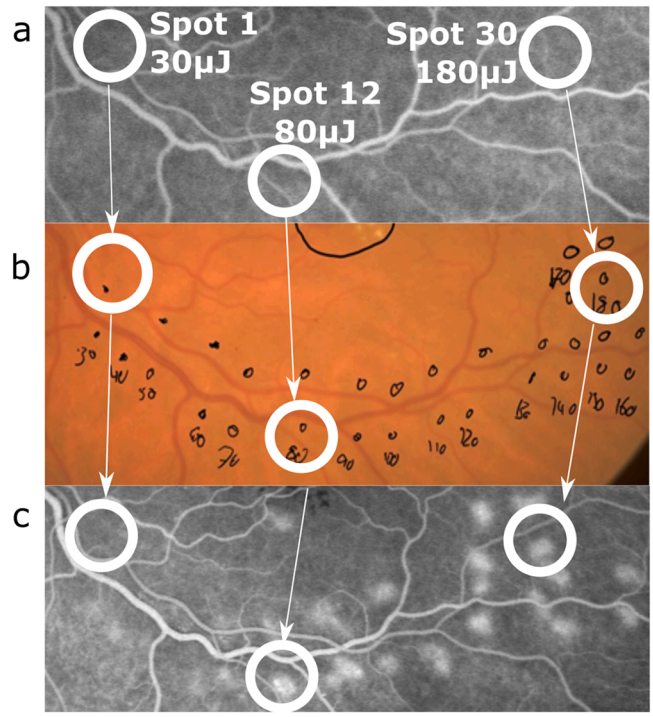

Fig. 4. Three diagnostic images of the same region. (a) FA image taken before irradiation, (b) Irradiation map pre treatment with spot location and additional information about applied pulse energy. (c) FA image taken 1 h after treatment. Circles and pointers identify selected irradiated regions (Spot 1, 12, and 30) in the three images. This includes a non-damaged region (spot 1), a FA-visible region (spot 12), and a region with ophthalmoscopically visible cell damage (spot 30).

was a mismatch between the documented spots (Fig. 4b) and FA-visible spots (Fig. 4c), FA information was labeled unknown for all spots of the treatment.

If no hyper-fluorescence was observable in a FA image taken before treatment (e.g. Fig. 4a Spot 12), and if cell damage was observable by hyper fluorescence in a FA image taken after treatment (e.g. Fig. 4c Spot 12) the spot was labeled as FA-positive. In the case of absence of hyper fluorescence, the spot was labeled as FA-negative (e.g. Fig. 4c Spot 1).

If it was not possible to distinguish a selective RPE lesion from its surroundings (e.g. due to intense pathological leakage), all transients of the entire treatment received the cell damage label unknown.

It is important to note that each spot can only have one cell damage classification. In the case of a FA-non-visible spot, all 15 pulses which were applied to a spot were classified as FA-nonvisible. In the case of FA-visible spots, it was not possible to know which pulses contributed to the corresponding visibility. Due to this attribution problem, the pulse with the highest laser pulse energy was used for FA-classification. This is also the pulse with the highest NL-value.

2.5. Performance metrics

The algorithm performance is expressed by the dependent statistical probabilities to correctly predict OA- and FA- labels (ground truth) by the NL or BL value.

The estimated dependent probabilities that a positive case (e.g. FA-visible) is identified correctly by the algorithm as a positive case is called sensitivity.

It is estimated by the ratio of the number of true positives (e.g. all green datapoints above the threshold line in Fig. 6a) and the number of all positives (e.g. all green datapoints in Fig. 6a).

The estimated dependent probabilities that a negative case is identified correctly by the algorithm as a negative case is called specificity. It is estimated by the ratio of the number of true negatives (e.g. all red datapoints below the threshold line in Fig. 6a) and the number of all negatives (e.g. all red datapoints in Fig. 6a).

If sensitivity and specificity are evaluated for a range of thresholds the resulting sensitivity-specificity pairs can be displayed in a x-y-curve. This x-y-curve is called the receiver operating characteristic (ROC) curve. The area under the ROC curve (AUC) [37] is a typical performance measure in classification problems. The optimization algorithm applied in this work was designed to maximize the AUC in the training set.

The threshold which is used by the algorithm for all datasets is determined by a values which merges sensitivity and specificity ($Y = sensitivity + specificity - 1$) [38]. The NL or BL -value leading to the highest Y in the development set is chosen as threshold value.

2.6. Data sets

When an algorithm is optimized on the base of an acquired dataset, there is the possibility to overfit it to dataset-individual datapoints. Increased differences in performance metrics indicate a loss of generalizability. The more datasets the more performance metric differences can be calculated. Due to the limited number of patients, a total number of 3 datasets were used in this work. Those were the training set the development set and the test set. The following explanation of the requirements for an assignment to a certain dataset is summarized in Table 1.

The training dataset consisted of fifteen treatments of twelve patients (nine CSCR, three DME). The data in this data set originated from treatment spots and test spots that could not be evaluated according to FA imaging (FA-classification unknown). Data from the training set was labeled with OA-transient information (OA positive/negative) only. The training dataset was the only dataset used for the automatic optimization process.

In the evaluation process, the performance metrics of the training dataset were compared to the development set. This set consisted of four treatments of three patients (two CSCR, one DME). Data in the development set originated from patients whose data was not applied for training. The data of the development set fulfilled the same criteria as the training set data.

Finally, the data from the test set originated from FA-evaluable test spots exclusively. This data was labeled with OA- and FA- information. Data from 11 treatments on 11 patients was included in the test set (nine CSCR, two DME).

3. Results

3.1. Overview

The training set consisted of 1847 pulses with MBF and 1414 pulses without. The development set consists of 770 pulses with MBF and 384 pulses without. The test set consists of 161 transients originating from FA hyper-fluorescent regions and 70 transients originating from FA non-hyper-fluorescent regions.

The parameter optimization for the training set found an optimum through the use of a bandpass filter with a high cutoff frequency of around 6 MHz and a low cutoff frequency of around 110 kHz. Additionally, the optimization procedure found a value of the algorithm variable $i = 11$ as best.

3.2. Necessity of pulse energy normalization

Fig. 3 shows a typical OA-transient (subfigure a, c) with the respective BL and NL values (subfigure b, d). It was observed that the energy dependence of the BL algorithm led to false decisions. The data in Fig. 5a and c originate from a treatment spot in the training set. In the scenario displayed in Fig. 5a and b, it can be observed that the baseline

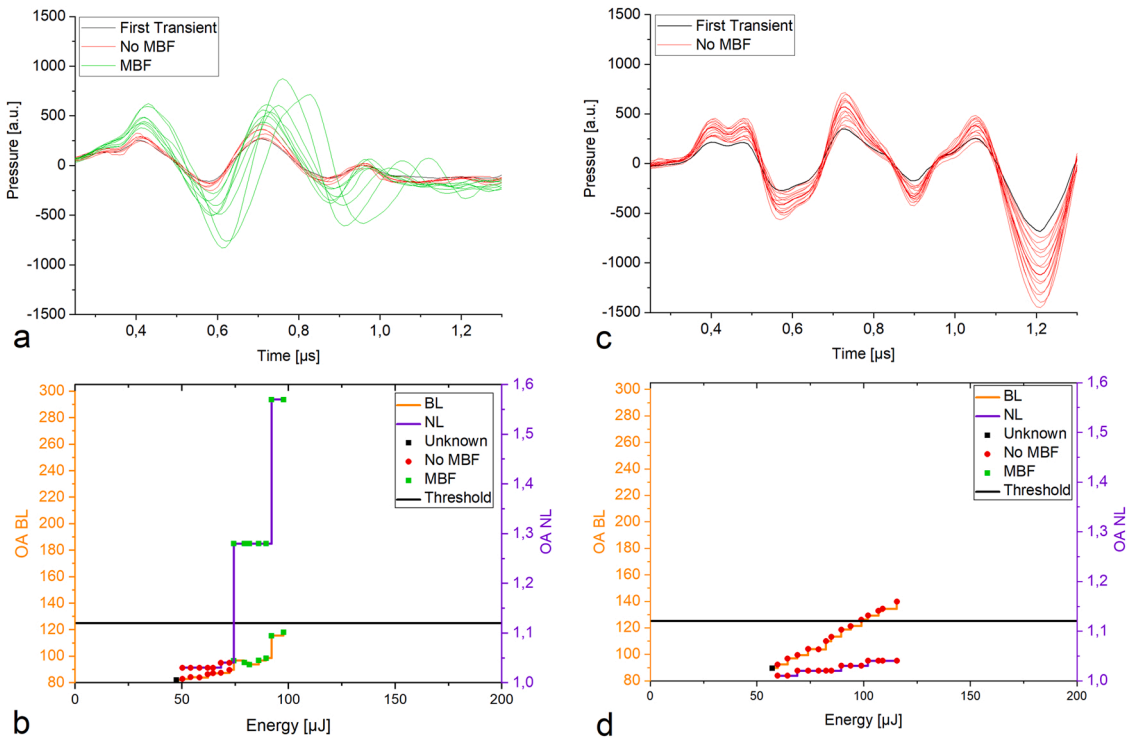

Fig. 5. Examples of NL and BL values of a spot above and below the MBF threshold. The black horizontal line shows the threshold value for the algorithms. (a) Displays pressure transients without any signs of microbubble formation (red) and with signs of microbubble formation. (green). (b) Displays the corresponding NL and BL-values from the data of subfigure a. The BL algorithm does not exceed its threshold value in subfigure b. This is a false negative decision. (c) Displays pressure transients without any signs of microbubble formation. (d) Displays NL and BL values from the data of subfigure c. The BL algorithm exceeds its threshold. This is a false positive decision.

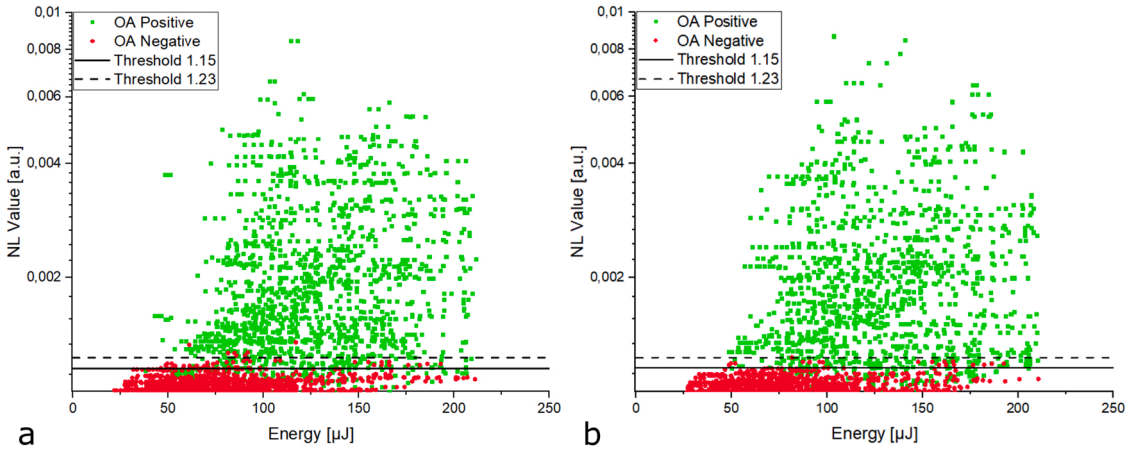

Fig. 6. Scatter plots of (a) training set and (b) Development set. Datapoints were labeled as OA negative or OA positive with respect to absence or presence of a nonlinear increase in pressure amplitude. The threshold of 1.15 leads to the highest Y in the development set. The threshold value of 1.23 leads to a specificity of 1 in the development set.

Table 1
Requirements for dataset-assignments.

	FA evaluable	OA evaluable	Symptom free area
Training Set	Not Required	Required	Not Required
Development Set	Not Required	Required	Not Required
Test Set	Required	Required	Required

method did not exceed its threshold value in the case of MBF. The low values of the acquired pressure transient were the cause for these low *BL* values.

In the scenario displayed in Fig. 5c and d, the baseline algorithm led to BL values above threshold while no signs of MBF can be found in the raw data (red colored transients only). It can also be observed that the *NL* values were not negatively influenced from the increase in laser pulse energy.

The ability to address the systematic error induced by the laser pulse energy increase makes the normalization procedure a necessity in the digital signal processing procedure.

3.3. Performance analysis

Regarding microbubble detection, the BL algorithm already achieved a sensitivity of 82% and a specificity of 98% in the test dataset at the threshold value of 125. The NL algorithm achieved a sensitivity of 96% and a specificity of 100%. Tables 1 and 2 summarize sensitivity and specificity for each dataset to detect microbubble formation in sensor data, and to predict FA visible damage.

Figs. 4(a and b) and 5 display the *NL* values for each spot. In Fig. 4a and b as well as 5b the colors indicate the presence (green) or absence (red) of microbubble formation. In Fig. 5a the colors indicate the presence or absence of cell damage (detected by fluorescence angiography). In all figures it can be easily seen that the laser pulse energy is not a good indicator for microbubble formation or cell damage.

Overlapping datapoints may make the presented scatterplots difficult to interpret. The scatterplots of Fig. 6b (cv set) and Fig. 7a (test set, FA labeling) were summarized in the ROC plot in Fig. 8. The black and blue marker indicate the performance (sensitivity/specificity pair) at thresholds of 1.15 and 1.23 respectively.

3.4. Generalizability results

The differences between training and development set express the generalizability of the performance metrics to detect microbubble induced characteristics in sensor data.

For the baseline algorithm sensitivity differences and specificity differences between training and development set reached values of 5% and 0.4% points. The sensitivity- and specificity-differences of the *NL* algorithm between training and development set were 3% and 0.6% points.

The difference between development set and FA-classified test set express the applicability of the particular optoacoustic value as an indicator for microbubble formation. BL sensitivity- and specificity- differences between development- and FA-set differ by values of 5% and 13% points. The *NL* sensitivity and specificity between development- and FA-set differ by values of 4% and 3% points.

3.5. False decisions

With regard to the BL algorithm, there were 22 false negative decisions and zero false positive decisions in the test dataset when a threshold value of 125 was applied. The pulse energy dependence was found to induce a systematic error (discussed in chapter 3.2). The NL algorithm was designed to remove this systematic error.

The NL algorithm led to zero false positive decisions and six false negative decisions in the test dataset when a threshold value of 1.15 was applied. In four out of six false-negative decisions made by the NL algorithm, the chosen pulse energy of the first pulse was so high that even the first pulse displayed signs of microbubble formation. In such a case the steep increase in optoacoustic amplitude, which happen at the transition for thermoelastic to thermo-mechanic cell damage, cannot be observed. The early microbubble formation was detected via comparisons with an optical feedback technique that is able to detect microbubbles by evaluating single pulses [25]. In the remaining two false negative decisions, the microbubble-associated characteristics in the sensor data occurred in the last one to two pulses only. The extent of microbubble-associated characteristics in the sensor data was minimal.

Table 2
Sensitivity and specificity at the best threshold achieved in the development set (BL $= 125$, NL $= 1.15$).

	BL		NL	
	Sensitivity	Specificity	Sensitivity	Specificity
Training (Sensor Data)	77%	87%	89%	96%
Development (Sensor Data)	82%	87%	92%	97%
Test (Sensor Data)	82%	98%	96%	100%
Test (FA Data)	86%	100%	96%	100%

4. Discussion

In early SRT studies, laser pulse energy settings were chosen with an energy titrating procedure including time consuming FA-imaging [39,40]. Then, optoacoustic microbubble monitoring techniques were applied [11]. Those techniques relied on multiple laser transients to detect microbubble formation. Later, optical approaches formation was applied to cease laser irradiation as soon as MBF was detected in in-vivo experiments [36,41]. and in clinical treatments [39].

While a single pulse microbubble detection was realized for optical MBF detection techniques, there is no approach for optoacoustic single transient microbubble detection. It was the goal of this study to develop an algorithm which can detect MBF by analyzing individual transients. The results have shown improved performance metrics of the NL- algorithm compared to the BL algorithm. Cell damage thresholds of the treated patients were already discussed in a previous work [25].

4.1. Baseline algorithm

An overfitting to dataset individual nuances can be detected by comparisons of performance measure differences between datasets. Since no optimization/fine-tuning has been done with the BL algorithm, low performance measure differences can be expected. Nevertheless, the performance measure differences are not zero. This raises the question of the origin of those differences. Although the optical properties of the eye have low influence on the acoustic signal, variability in the acoustic coupling (contact lens to eye) and the angular dependence of the acoustic signal can still influence acquired transients [33]. Statistical fluctuations induced by those influences can be assumed to be the origin of the observed differences.

4.2. NL algorithm

The acoustic pressure acquired by the ultrasonic transducer is proportional to the material specific Grüneisen coefficient and the laser pulse energy. The NL- algorithms also include normalization procedures that eliminate the direct influence of the laser pulse energy increase on the calculated values. In the case of a constant Grüneisen coefficient the *NL* values should be independent of the laser pulse energy. This can be seen best in the low increase in the NL values in the regime below microbubble formation in Fig. 5. The existence of a low increase in NL values in the regime below threshold originates from changing signal-to-noise levels of the evaluated transients. This phenomenon could be reduced if the signal-to-noise ratio could be improved.

Most false negative decision made by the NL algorithm share the commonality that even the first pulse of the ramp leads to microbubble formation. This usually leads to decreased NL values and consequently to false negative decisions. In practice, this can be avoided by starting a pulse energy for the first irradiation and repeatedly increase the pulse energy until the microbubble detection occurs within the irradiation

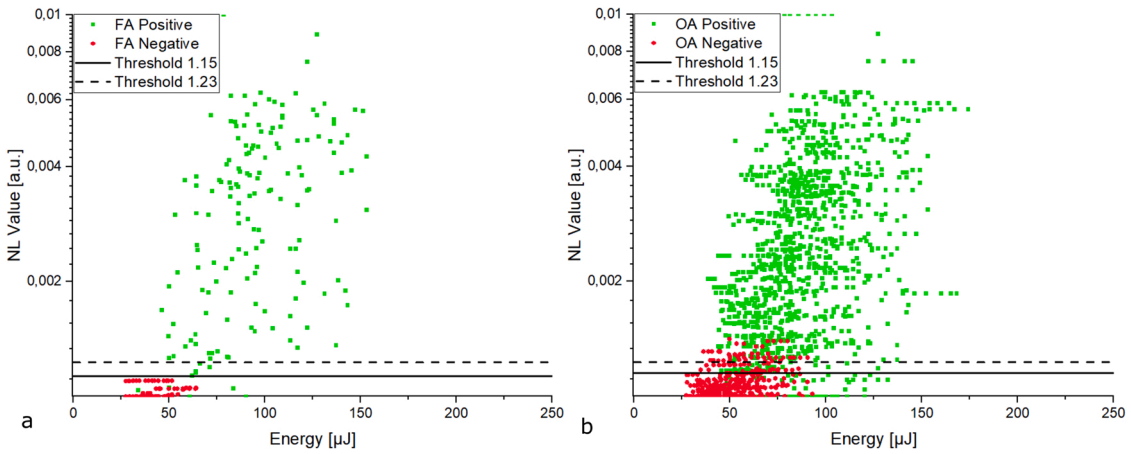

Fig. 7. (a) Scatter plot with cell damage labels. Datapoints were labeled as FA negative or FA positive with respect to the visibility of hyperfluorescent regions in FA images. (b) Scatter plot with microbubble classification labels. Datapoints were labeled as OA negative or OA positive with respect to absence or presence of a nonlinear increase in pressure amplitude. The threshold of 1.15 leads to the highest Y in the development set. The threshold value of 1.23 leads to a specificity of 1 in the development set.

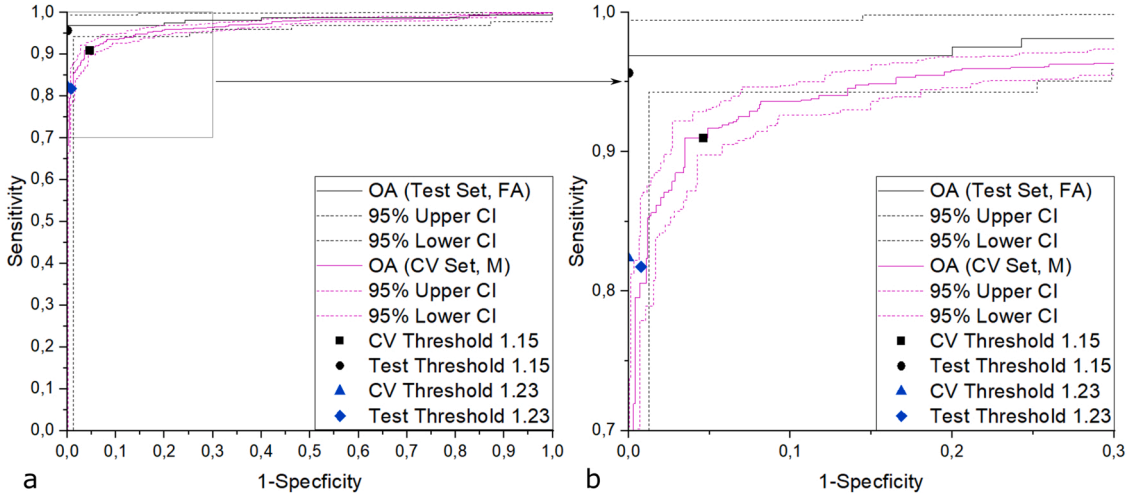

Fig. 8. ROC Curve of Fig. 6b (NL algorithm, cv set) and Fig. 7a (NL algorithm, test set, FA labeling). The threshold of 1.15 is indicated with black markers 1.23 is indicated with blue markers. The dotted lines indicate the 95% confidence interval.

time. Further false negative cases had a low SNR. An improvement of the sensor-sensitivity or an improvement of the analog amplification would lead to fewer false decisions of this type.

Knowledge about the state of MBF in the first pulse can be gained through an optical feedback mechanism [25]. Hence, it can be hypothesized that a combination of the optoacoustic feedback techniques with an optical feedback technique would improve performance. It may also be speculated whether the performance metrics in retreatments are different than those in initial treatments. Hyperpigmentation in irradiated regions was observed in vivo 2 and 4 weeks after treatment [7]. The changes in pigmentation may influence the radiant exposure thresholds of retreatments. Nevertheless, an algorithm would still be able to detect microbubble formation. Furthermore, there is no increased number of false positive or false negative retreatment irradiations in any dataset.

It may also be speculated that very early stages of microbubble formation may be undetected by the opto-acoustic approach. If this is the case, those bubbles did induce any damage which was detectable via fluorescence angiography.

4.3. Working-point range

It can be speculated that, with a very precise microbubble detection and irradiation ceasing, too few RPE cells may get affected to induce a therapeutic effect. Thus, it may be reasonable to exceed the threshold of initial microbubble detection.

In this scenario it is essential to know by how much the threshold can be exceeded before extended cell damage is induced. To estimate this range, dose response methods were applied to evaluate the effective dose for a 16% chance (ED16) of ophthalmoscopically visible cell damage and an 86% chance (ED86) for FA visible cell damage.

Probit plots were commonly used in former studies on SRT. The dataset consists of an independent variable and a binary variable. The effective dose (ED) at which there is a 16% or 86% probability to achieve an effect is calculated via the fitted function.

Published SRT studies made use of the laser pulse energy or the radiant exposure as the independent variable. However, this does not consider the support of MBF techniques, which removes uncertainties induced by inter- and intraindividual variations of the local MBF threshold.

To consider MBF techniques each laser pulse energy is set into relation to an eye individual threshold for bubble formation (mean of MBF thresholds within an eye) [25]. To do this, a ratio (δ) of the pulse energy and the respective eye-individual MBF threshold was calculated.

With this δ a probit evaluation of FA visibility and ophthalmoscopic

visibility was performed. When microbubble detection was done with the NL algorithm the lower 95% confidence interval of the ED16 value for ophthalmoscopic visibility exceeds the upper 95% confidence interval for ED86 for FA visibility by a factor of 1.98.

To be safe this entire range should not be used. If doubts of the therapeutic effect of SRT treatments arise, the threshold pulse energy may be exceeded by a lower factor (e.g. 1.2).

Iterative irradiation prior to the threshold of MBF are unlikely to have a noteworthy effect since affected RPE in the region of peak temperature are disrupted. This makes any other effect irrelevant, which would happen to the cell otherwise. As it has been reported, at pulse durations shorter than 2 μs, MBF is the initial mechanism for cell damage [5,42,43]. At the point of MBF, neighboring cells experience an increase in temperature [44].

A repetition rate of 100 Hz with 1.7 μs lowers the heat accumulation [35]. However, even repetition rates of 500 Hz and 5 μs having a higher heat accumulation led to selective cell damage in the RPE, if the laser spot diameter is kept very small for faster heat diffusion [16,45]. Whether other biological effects like the expression of heat shock proteins is a point of debate.

4.4. Limitations of this study

The optimization process was performed for only 15 eyes (10 were evaluable by FA imaging). The treatment protocol, which was needed to be followed to ensure a safe and effective treatment, introduced a higher number of FA-visible and OA-positive spots compared to FA-nonvisible and OA-negative spots. More data, especially more FA-nonvisible and ophthalmoscopically-visible data, is required to improve the statistical evaluation.

5. Conclusion

It could be shown in this work using clinical data that appropriate optoacoustic based algorithms are able to detect laser induced cell damage with a sensitivity of 96% and a specificity of 100% during retinal exposure with a series of μs laser pulses in SRT. An algorithm considering the dependence of the acoustic pressure on the laser pulse energy as a normalization performs superior to a baseline algorithm without this feature.

There are different scenarios for clinical translation. This algorithm can be used in treatment guidance where the treating clinician decides how much energy is applied and the algorithm displays whether microbubble formation took place and with which spot in the ramp MBF was achieved first.

Final aim is a fully automatic irradiation where the clinician just chooses the location on the retina and releases the laser firing. The algorithm ceases the pulse energy ramp after MBF formation took place (or one or two pulses above first MBF is noticed to guarantee MBF on the whole area) and thus reduced the overall energy applied to the retina.

The *NL* algorithm may be combined with an optical microbubble detection method, to be able to detect microbubble at the very first pulse as well and as a backup system in general.

Microbubble detection methods are expected to increase safety as knowledge is gained about the local MBF threshold and efficiency through a reduction of the number of retreatments owing to undertreatments.

Disclosures

Ralf Brinkmann is inventor of patents, which are hold by the Medizinisches Laserzentrum Lübeck GmbH and licensed to commercial entities that are related to the technology and analysis methods described in this study. Data were acquired and processed from patients by coauthors unaffiliated with any commercial entity.

Declaration of Competing Interest

The authors declare the following financial interests/personal relationships which may be considered as potential competing interests: Ralf Brinkmann is inventor of patents, which are hold by the Medizinisches Laserzentrum Lübeck GmbH and licensed to commercial entities that are related to the technology and analysis methods described in this study. Data were acquired and processed by coauthors unaffiliated with any commercial entity.

Acknowledgements

We thank Lutronic Inc. (Republic of Korea) for resourcing the RGEN Laser Systems. The algorithm implemented in the R:GEN system was not used clinically, nor considered, nor evaluated in this work.

References

[1] Gabel, Birngruber, Hillenkamp, Visible and near infrared light absorption in pigment epithelium and choroid, in: Proceedings of 23rd Consilium Ophthalmologicum, Kyoto Excerpta Medica 450 (1978) 658–662.
[2] D.H. Sliney, J. Marshall, Tissue specific damage to the retinal pigment epithelium: mechansims and therapeutic implications, Lasers Light Ophthalmol. 5 (1) (1992) 17–28.
[3] C. Framme, G. Schuele, J. Roider, D. Kracht, R. Birngruber, R. Brinkmann, Threshold determinations for selective retinal pigment epithelium damage with repetitive pulsed microsecond laser systems in rabbits, Ophthalmic Surg. Lasers 33 (5) (2002) 400–409.
[4] R. Birngruber, F. Hillenkamp, V.P. Gabel, Theoretical investigations of thermal retinal injury, Health Phys. 48 (8) (1985) 781–796.
[5] R. Brinkmann, G. Huettmann, J. Roegener, J. Roider, R. Birngruber, C.P. Lin, Origin of retinal pigment epithelium cell damage by pulsed laser irradiance in the nanosecond to microsecond time regimen, Lasers Surg. Med. 27 (5) (2000) 451–464.
[6] C.P. Lin, M.W. Kelly, Cavitation and acoustic emission around laser-heated microparticles, Appl. Phys. Lett. 72 (22) (1998) 2800–2802.
[7] J. Roider, N.A. Michaud, T.J. Flotte, R. Birngruber, Response of the retinal pigment epithelium to selective photocoagulation, Arch. Ophthalmol. 110 (1992), 1786-1786.
[8] C. Framme, A. Walter, L. Berger, P. Prahs, C. Alt, D. Theisen-Kunde, J. Kowal, R. Brinkmann, Selective retina therapy in acute and chronic-recurrent central serous chorioretinopathy, Ophthalmologica 234 (4) (2015) 177–188.
[9] S. Kang, Y.G. Park, J.R. Kim, E. Seifert, D. Theisen-Kunde, R. Brinkmann, Y.J. Roh, Selective retina therapy in patients with chronic central serous chorioretinopathy: a pilot study, Medicine 95 (3) (2016), e2524.
[10] C. Klatt, M. Säger, T. Oppermann, E. Pörksen, F. Treumer, J. Hillenkamp, E. Fritzer, R. Brinkmann, R. Birngruber, J. Roider, Selective retina therapy for acute central serous chorioretinopathy, Br. J. Ophthalmol. 95 (1) (2011) 83–88.
[11] A. Yasui, M. Yamamoto, K. Hirayama, K. Shiraki, D. Theisen-Kunde, R. Brinkmann, Y. Miura, T. Kohno, Retinal sensitivity after selective retina therapy (SRT) on patients with central serous chorioretinopathy, Graefes Arch. Clin. Exp. Ophthalmol. 255 (2) (2017) 243–254.
[12] J. Roider, S.H.M. Liew, C. Klatt, H. Elsner, E. Pörksen, J. Hillenkamp, R. Brinkmann, R. Birngruber, Selective retina therapy (SRT) for clinically significant diabetic macular edema, Graefes Arch. Clin. Exp. Ophthalmol. 248 (9) (2010) 1263–1272.
[13] Y.G. Park, J.R. Kim, S. Kang, E. Seifert, D. Theisen-Kunde, R. Brinkmann, Y.J. Roh, Safety and efficacy of selective retina therapy (SRT) for the treatment of diabetic macular edema in Korean patients, Graefes Arch. Clin. Exp. Ophthalmol. 254 (9) (2016) 1703–1713.
[14] Boergen Birngruber, Gabel Drechsel, Welsch Hillenkamp, Lund, Untersuchungen zur Lichtabsorption am Auge, Ges. Strahl. Umweltforsch. mbH München 277 (1978) 1–22.
[15] E.A. Boettner, J.R. Wolter, Transmission of the ocular media, Investig. Ophthalmol. Vis. Sci. 1 (6) (1962) 776–783.
[16] Hillenkamp Roider, Birngruber Flotte, Microphotocoagulation: selective effects of repetitive short laser pulses, Proc. Natl. Acad. Sci. USA 90 (18) (1993) 8643–8647.
[17] R.G. Borland, D.H. Brennan, J. Marshall, J.P. Viveash, The role of fluorescence angiography in the detection of laser-induced damage to the retina: a threshold study for Q-switched, neodymium and ruby lasers, Exp. Eye Res. 27 (1978) 471–493.
[18] Puliafito Birngruber, Lin Gawande, Fujimoto Schoenlein, Femtosecond laser-tissue interactions: retinal injury studies, IEEE J. Quantum Electron. 23 (10) (1987) 1836–1844.
[19] J. Roider, F. Hillenkamp, T. Flotte, R. Birngruber, Microphotocoagulation: selective effects of repetitive short laser pulses, Proc. Natl. Acad. Sci. USA 90 (18) (1993) 8643–8647.
[20] M.P. Lopez-Saez, E. Ordoqui, P. Tornero, A. Baeza, T. Sainza, J.M. Zubeldia, M. L. Baeza, Fluorescein-induced allergic reaction, Ann. Allergy Asthma Immunol. 81 (5) (1998) 428–430.

[21] D.F. Marcus, J.A. Bovino, D. Williams, Adverse reactions during intravenous fluorescein angiography, Arch. Ophthalmol. 102 (6) (1984) 825.
[22] C. Alt, C. Framme, S. Schnell, H. Lee, R. Brinkmann, C.P. Lin, Selective targeting of the retinal pigment epithelium using an acousto-optic laser scanner, J. Biomed. Opt. 10 (6) (2005), 064014.
[23] S. Zbinden, S.S. Kucur, P. Steiner, S. Wolf, R. Sznitman, Automatic assessment of time-resolved OCT images for selective retina therapy, Int. J. Comput. Assist. Radiol. Surg. 11 (6) (2016) 863–871.
[24] P. Steiner, A. Ebneter, L.E. Berger, M. Zinkernagel, B. Povazay, C. Meier, J. H. Kowal, C. Framme, R. Brinkmann, S. Wolf, et al., Time-resolved ultra-high resolution optical coherence tomography for real-time monitoring of selective retina therapy, Investig. Ophthalmol. Vis. Sci. 56 (11) (2015) 6654–6662.
[25] E. Seifert, J. Tode, A. Pielen, D. Theisen-Kunde, C. Framme, J. Roider, Y. Miura, R. Birngruber, R. Brinkmann, Selective retina therapy: toward an optically controlled automatic dosing, J. Biomed. Opt. 23 (11) (2018) 1–12.
[26] J. Neumann, R. Brinkmann, in: S.L. Jacques, D.D. Duncan, S.J. Kirkpatrick, A. Kriete (Eds.), Microbubble Dynamics around Melanosomes Irradiated with Microsecond Pulses, SPIE, 2002, pp. 180–186.
[27] J. Neumann, R. Brinkmann, Nucleation dynamics around single microabsorbers in water heated by nanosecond laser irradiation, J. Appl. Phys. 101 (11) (2007), 114701.
[28] J. Neumann, R. Brinkmann, Self-limited growth of laser-induced vapor bubbles around single microabsorbers, Appl. Phys. Lett. 93 (3) (2008), 033901.
[29] J. Neumann, R. Brinkmann, Interferometric detection of laser-induced microbubbles in the retinal pigment epithelium, in: R. Birngruber, H. van den Bergh (Eds.), European Conferences on Biomedical Optics, Laser-Tissue Interactions, Therapeutic Applications, and Photodynamic Therapy, SPIE Proceedings, Munich, 2001, pp. 81–86.
[30] Y.G. Park, E. Seifert, Y.J. Roh, D. Theisen-Kunde, S. Kang, R. Brinkmann, Tissue response of selective retina therapy by means of a feedback-controlled energy ramping mode, Clin. Exp. Ophthalmol. 42 (9) (2014) 846–855.
[31] H. Lee, C. Alt, C.M. Pitsillides, C.P. Lin, Optical detection of intracellular cavitation during selective laser targeting of the retinal pigment epithelium: dependence of cell death mechanism on pulse duration, J. Biomed. Opt. 12 (6) (2007), 064034.
[32] D. Kaufmann, C. Burri, P. Arnold, V.M. Koch, C. Meier, B. Povazay, J. Justiz, Selective retina therapy enhanced with optical coherence tomography for dosimetry control and monitoring: a proof of concept study, Biomed. Opt. Express 9 (7) (2018) 3320–3334.
[33] G. Schüle, H. Elsner, C. Framme, J. Roider, R. Birngruber, R. Brinkmann, Optoacoustic real-time dosimetry for selective retina treatment, J. Biomed. Opt. 10 (6) (2005), 064022.
[34] M.W. Sigrist, F.K. KneubÃ¼hl, Laser-generated stress waves in liquids, J. Acoust. Soc. Am. 64 (6) (1978) 1652–1663.
[35] G. Schule, G. Huttmann, C. Framme, J. Roider, R. Brinkmann, Noninvasive optoacoustic temperature determination at the fundus of the eye during laser irradiation, J. Biomed. Opt. 9 (1) (2004) 173–179.
[36] K. Minhee, Y.G. Park, S. Kang, Y.J. Roh, Comparison of the tissue response of selective retina therapy with or without real-time feedback-controlled dosimetry, Graefes Arch. Clin. Exp. Ophthalmol. 256 (9) (2018) 1639–1651.
[37] A.P. Bradley, The use of the area under the roc curve in the evaluation of machine learning algorithms, Pattern Recogn. 30 (7) (1997) 1145–1159.
[38] W.J. Youden, Index for rating diagnostic tests, Cancer 3 (1) (1950) 32–35.
[39] Y.G. Park, S. Kang, M. Kim, N. Yoo, Y.J. Roh, Selective retina therapy with automatic real-time feedback-controlled dosimetry for chronic central serous chorioretinopathy in Korean patients, Graefes Arch. Clin. Exp. Ophthalmol. 255 (7) (2017) 1375–1383.
[40] C. Framme, A. Walter, P. Prahs, R. Regler, D. Theisen-Kunde, C. Alt, R. Brinkmann, Structural changes of the retina after conventional laser photocoagulation and selective retina treatment (SRT) in spectral domain OCT, Curr. Eye Res. 34 (7) (2009) 568–579.
[41] E. Seifert, Y.-J. Roh, A. Fritz, Y.G. Park, S. Kang, D. Theisen-Kunde, R. Brinkmann, Automatic irradiation control by an optical feedback technique for selective retina treatment (SRT) in a rabbit model, in: European Conference on Biomedical Optics, Medical Laser Applications and Laser-Tissue Interactions VI, Optical Society of America, Munich, 2013, p. 880303.
[42] G. Schuele, M. Rumohr, G. Huettmann, R. Brinkmann, RPE damage thresholds and mechanisms for laser exposure in the microsecond-to-millisecond time regimen, Investig. Ophthalmol. Vis. Sci. 46 (2) (2005) 714–719.
[43] E. Seifert, S.R. Sonntag, P. Kleingarn, D. Theisen-Kunde, S. Grisanti, R. Birngruber, Y. Miura, R. Brinkmann, Investigations on retinal pigment epithelial damage at laser irradiation in the lower microsecond time regime, Investig. Ophthalmol. Vis. Sci. 62 (3) (2021) 32.
[44] R. Brinkmann, G. Hüttmann, J. Rögener, J. Roider, R. Birngruber, C.P. Lin, Origin of retinal pigment epithelium cell damage by pulsed laser irradiance in the nanosecond to microsecond time regimen, Lasers Surg. Med. 27 (5) (2000) 451–464.
[45] Michaud Roider, Birngruber Flotte, Response of the retinal pigment epithelium to selective photocoagulation, Arch. Ophthalmol. 110 (1992), 1786-1786.

Eric Seifert received a master of science in photonics at Aalen University. He worked for over 9 years at the Medical Laser Center Lübeck GmbH and (co)authored several papers and conference proceedings on Selective Retina Therapy and other topics on retinal laser treatment.

Jan Tode, M.D., is ophthalmologist at the department of ophthalmology at University of Kiel. He studied medicine at the University of Kiel and Bialystock (Poland). He completed his ophthalmological training in 2016. He is head of the murine experimental laboratory at the department. His research focusses on translational examinations for the evaluation of new therapeutic aspects in the treatment of uveitis and degenerative retinal diseases.

Amelie Pielen, M.D. habil. is ophthalmologist at the University Eye Hospital of Hannover Medical School (MHH). She studied medicine at the University of Bonn, Perugia (Italy), Adelaide (Australia) and Freiburg. She completed her training in ophthalmology in 2010 at Freiburg and joined Prof. Framme`s Team at MHH in 2013. Her research focusses on medical and surgical retina, imaging and SRT.

Dirk Theisen-Kunde studied Engineering at the Polytechnic University Lübeck (Germany) and Physics at the University of Loughborough (UK). He worked 6 years at the Institute of Biomedical Optics at the University of Lübeck in the field of endoscopic laser surgery. Since 2010 he is CTO at the Medical Laser Center Lübeck GmbH and responsible for clinical prototyping of medical devices. His R&D focuses mainly on ophthalmology and laser surgery.

Carsten Framme, M.D., M.B.A., is professor and chairman of ophthalmology at the Medical School of Hannover (MHH) in Germany since 2012. He studied medicine at the MHH and was clinically trained in Lübeck, Regensburg and Bern (Switzerland). He did a research fellowship at the Medical Laser Center in Lübeck and at the Wellman Laboratories of Photomedicine in Boston. His research focuses on retinal laser medicine as well as on drug-tissue interactions and surgical approaches.

Johann Roider, M.D., is a professor of ophthalmology. He studied mathematics, physics, and medicine at Munich universities, Germany. He did a research fellowship at the Wellman Laboratories of Photomedicine, Boston. His clinical training was obtained at the universities of Lübeck and Regensburg. Since 2002 he has been the chairman of the Department of Ophthalmology, University of Kiel. His research focuses are laser–tissue interactions and vitreoretinal disorders.

Yoko Miura studied medicine in Osaka, Japan, and received a medical license in 1997 and Ph.D. in 2002. After working in the Osaka City University Hospital till 2006, she engaged in basic research at the University Eye Clinic in Kiel till 2009. She received a German medical license in 2012, and today is a faculty member at the Institute of Biomedical Optics and an Ophthalmologist and at the Department of Ophthalmology at University of Luebeck.

Reginald Birngruber studied electrical engineering and physics and graduated in physics (Ph.D.) and in medical biophysics (M.D. habilis) in Germany. After his retirement from CEO and CRO of the Medical Laser Center Lübeck and the chair of the Institute of Biomedical Optics, he now makes his expertise and contacts available to colleagues in Lübeck and Boston. Current activities include mechanisms of laser tissue effects, optical tissue diagnostics, laser therapy control and new therapeutic techniques.

Ralf Brinkmann studied physics at the University of Hannover, Germany, with a focus on quantum optics and lasers. After a 5-year industrial interim period, he joined the Medical Laser Center in Lübeck, Germany, in 1993, and received his Ph.D. from the University of Lübeck. Since 2005 he has been holding a permanent position as a faculty member at the University Institute of Biomedical Optics, and is also leading the Medical Laser Center as CEO.